Heterotypic gap junction channels as voltage-sensitive valves for intercellular signaling

Nicolas Palacios-Prado and Feliksas F. Bukauskas[1]

Dominick P. Purpura Department of Neuroscience, Albert Einstein College of Medicine, Bronx, NY 10461

Edited by Michael V. L. Bennett, Yeshiva University, New York, NY, and approved July 9, 2009 (received for review February 23, 2009)

Gap junction (GJ) channels assembled from connexin (Cx) proteins provide a structural basis for direct electrical and metabolic cell–cell communication. By combining fluorescence imaging and dual whole-cell voltage clamp methods, we demonstrate that in response to transjunctional voltage (V_j) Cx43/Cx45 heterotypic GJs exhibit both V_j-gating and dye transfer asymmetries. The later is affected by ionophoresis of charged fluorescent dyes and voltage-dependent gating. We demonstrate that small differences in resting (holding) potentials of communicating cells can fully block (at relative negativity on Cx45 side) or enhance (at relative positivity on Cx45 side) dye transfer. Similarly, series of high frequency V_j pulses resembling bursts of action potentials (APs) can fully block or increase the transjunctional flux (J_j) of dye depending on whether pulses are generated in the cell expressing Cx43 or Cx45, respectively. Asymmetry of J_j-V_j dependence is enhanced or reduced when ionophoresis and V_j-gating act synergistically or antagonistically, whereas single channel permeability (P_γ) remains unaffected. This modulation of intercellular signaling by V_j can play a crucial role in many aspects of intercellular communication in the adult, in embryonic development, and in tissue regeneration.

connexin | intercellular permeability | voltage gating | dye transfer | fluorescent proteins

Gap junction (GJ) channels span the plasma membranes of adjacent cells and are formed by the docking of two hemichannels (connexons) oligomerized from connexin (Cx) proteins, which consist of 21 distinct isoforms (1). GJ channels formed from a single Cx isoform are called homotypic, whereas those formed between cells expressing different Cx isoforms are called heterotypic. GJs provide a direct pathway for cell-to-cell electrical signaling and metabolic communication, allowing the passage of small ions, amino acids, metabolites, tetraethylammonium and signaling molecules such as cAMP, IP_3, siRNA and small peptides ((2–5) and reviewed in ref. 6).

Earlier studies have shown that heterotypic junctions in which a Cx45 is paired with Cx31, Cx40 or Cx43 exhibit a strong voltage-gating asymmetry and modulatable cell-to-cell electric signaling from nearly uni-directional to bidirectional (7–9). Cx45 is expressed in a variety of tissues, but most abundantly in cardiovascular and nervous systems (1, 10). Blood vessels express Cx37, Cx40, Cx43 and Cx45, with the most abundant expression of Cx37 and Cx40 in endothelial cells and Cx43 and Cx45 in smooth muscle cells (11, 12). Thus, heterotypic GJs containing Cx45 can be formed between smooth muscle cells as well as between smooth muscle and endothelial cells. Furthermore, Cx45 may form junctions with mCx30.2, Cx40 and Cx43 in the heart between cardiomyocytes or cardiomyocytes and fibroblasts (13), between neurons with mCx30.2 and Cx36 (14) and between astrocytes and neurons with Cx43 (15). Here, we show that the V_j initiated by small voltage steps or high frequency activity on one side of Cx43/Cx45 heterotypic junctions can substantially modulate metabolic communication and that these heterotypic junctions may act as voltage-sensitive regulatory valves for intercellular signaling.

Results

Voltage-Gating and Signaling Asymmetry. We examined voltage-gating and cell-to-cell signaling asymmetry using a dual whole cell voltage clamp method as previously described (9) between HeLa cells expressing Cx43 or Cx43-EGFP (cell-1) and those expressing Cx45, Cx45-CFP or Cx45-EGFP (cell-2) and forming heterotypic junctions. Fig. 1*A* shows a fluorescence image of a HeLaCx43-EGFP/HeLaCx45-CFP cell pair, in which the steady-state conductance (g_j) dependence on transjunctional voltage (V_j), was recorded by applying slow (1 mV/s) V_j ramps to Cx43-expressing cell and measuring transjunctional current (I_j) (see Fig. 1*B*). The observed g_j-V_j dependence had a peak of g_j at $V_j \approx$-25 mV and demonstrated strong V_j-gating asymmetry. The reduction of g_j at positive V_js is caused by the closure of Cx45 hemichannels that gate at relative negativity on their cytoplasmic side, whereas the reduction in g_j for negative V_js result from closure of Cx43 hemichannels that also gate at relative negativity but are less V_j sensitive than Cx45 hemichannels (7). It was proposed that the ≈3.5-fold lower conductance of the Cx45 hemichannel causes a higher fraction of V_j to drop across it resulting in an enhanced V_j-gating sensitivity of the Cx45 hemichannel and reduced V_j-gating sensitivity of the Cx43 hemichannel (9, 16). All 64 Cx43/Cx45 cell pairs examined demonstrated V_j-gating asymmetry comparable to that shown in Fig. 1*B*. Similar V_j-gating asymmetry was reported for Cx31/Cx45 (8) and Cx40/Cx45 (9) junctions.

Earlier, it was shown that V_j-gating asymmetry in Cx43/Cx45 junctions can cause asymmetry of electrical signal transfer, which can be effectively modulated by the difference in holding potentials between the cells (ΔV_h) (7). Fig. 1*C* shows an experiment in which the Cx45-expressing cell (cell-1) was initially voltage clamped to −12 mV and repeated (5 Hz) 100 ms and 90 mV V_j pulses of positive and negative polarity were applied. Evoked coupling potentials were recorded in the Cx43-expressing cell (cell-2) maintained in current clamp mode. Positive pulses were effectively transferred to cell-2, whereas transfer of negative pulses was greatly attenuated. Transfer of negative pulses gradually decreased presumably due to gradual g_j decrease. After increases in the V_h of cell-1 (from −12 to 0 and to +12 mV; see red arrows), responses in cell-2 progressively become more symmetric (see *Insets* 1, 2 and 3 in Fig. 1*C*). Therefore, cells demonstrate electrical signal transfer asymmetry, which can be modulated from virtually unidirectional to bidirectional by relatively small changes in ΔV_h. Changes in the duration of the pulses from 5 to 100 ms, while maintaining interpulse interval equal to the duration of the pulse, resulted in similar signal transfer asymmetry that we observed in all 24 Cx43/Cx45 cell

Author contributions: N.P.-P. and F.F.B. designed research, performed research, analyzed data, and wrote the paper.

The authors declare no conflict of interest.

This article is a PNAS Direct Submission.

[1]To whom correspondence should be addressed. E-mail: fbukausk@aecom.yu.edu.

This article contains supporting information online at www.pnas.org/cgi/content/full/0901923106/DCSupplemental.

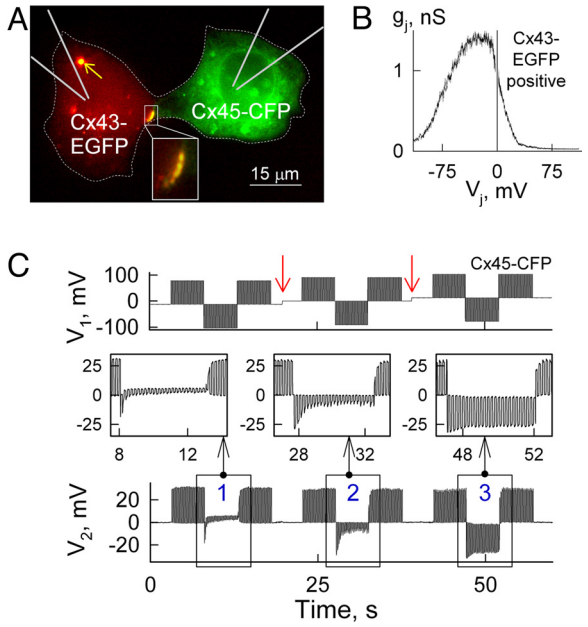

Fig. 1. V_j-gating and modulation of electrical signaling asymmetry. (*A*) Fluorescence image of a HeLaCx43-EGFP/HeLaCx45-CFP cell pair exhibiting a heterotypic junctional plaque (JP; see *Inset*). An internalized heterotypic JP is shown by the arrow. (*B*) g_j-V_j dependence measured in the cell pair shown in *A* by applying slow (1 mV/s) V_j ramps, demonstrates voltage-gating asymmetry. (*C*) Modulation of intercellular electric signaling asymmetry in the cell pair shown in *A*. V_1 and V_2 traces show the voltage protocol applied to HeLaCx45-CFP (cell-1) and the electrotonic potentials measured in HeLaCx43-EGFP (cell-2), respectively. Red arrows indicate a 12 mV increase of the holding potential in cell-1 starting from −12 mV and going to 0 mV and then to 12 mV (*Bottom Insets* 1, 2 and 3, respectively).

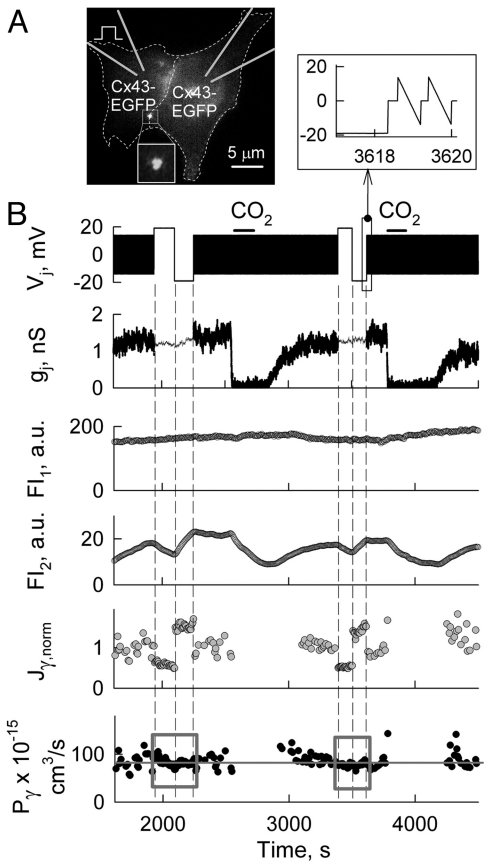

Fig. 2. Dye transfer modulation by ionophoretic effect of V_j in the absence of V_j-gating. (*A*) Fluorescence image of a HeLaCx43-EGFP cell pair exhibiting a single JP (see *Inset*). (*B*) Simultaneous electrophysiological and fluorescence imaging recordings in the cell pair shown in *A*. The V_j trace shows the voltage protocol applied to cell-1 loaded with AF^{350} (see diagram in *A*). Repeated V_j ramps of ± 15 mV applied in cell-1 were used to measure I_j in between V_j steps of ± 20 mV (see expanded traces in the *Top-Right Inset*). FI_1 and FI_2 traces show dynamics of dye fluorescence in cell-1 and cell-2, respectively. $J_{\gamma,norm}$ and P_γ traces show single channel flux normalized to the control value, and single channel permeability, respectively. On average, at $V_j \approx 0$ mV, $P_\gamma = \approx 83 \pm 5 \times 10^{-15}$ cm^3/s (gray line). Two consecutive applications of CO_2 (horizontal bars) were used to block GJs and calculate averaged P_p ($P_p = 1.3 \times 10^{-11}$ cm^3/s).

pairs examined. A similar phenomenon was reported in amphibian blastomeres exhibiting a small offset in resting potentials (17).

Dye Transfer Modulation by Transjunctional Voltage. Earlier studies have documented that GJs are permeable to second messengers, such as Ca^{2+}, cAMP and IP_3 in a Cx type dependent manner (6). Compared with Cx32, Cx43 GJs demonstrate ≈15-fold higher permeability for metabolites such as glutamate, glutathione, ADP and AMP, and ≈10-fold lesser permeability to adenosine (18). Ionic forms of all the above-mentioned molecules are comparable in molecular mass and net charge with Alexa Fluor-350 (326 Da, z = −1) and Lucifer Yellow (443 Da, z = −2) used in our studies. We did not assess permeability to positively charged dyes because of their strong binding to nucleic acids.

To determine the direct effect of transjuctional electrical field on the cell-to-cell transfer of dye molecules, we performed electrophysiological and fluorescence imaging studies in HeLaCx43-EGFP cell pairs (Fig. 2*A*), which exhibited almost no V_j-gating over ± 20 mV V_j steps. Cell-1 (Cx43-EGFP) was patched with the pipette containing Alexa Fluor-350 (AF^{350}). After both cells were transferred to whole-cell voltage-clamp mode, fluorescence intensity (FI) of AF^{350} in cell-1 and cell-2 approached a steady state. Then CO_2 was applied twice to block GJs. To measure I_j and g_j, repeated small voltage ramps were applied to cell-1. In between repeated ramps, two series of V_j steps of ± 20 mV were applied to cell-1. The amplitude and duration of the steps were too small to induce V_j-gating and reduction in g_j, whereas FI_2 showed changes due to the direct effect of V_j on AF^{350} transfer. We and others assumed that when the concentration of dye is <1 mM, dye concentration (C) is directly proportional to FI, C = k(FI), where k is a constant (19, 20). The total transjunctional flux (J_j) of dye when both patch pipettes are in the whole-cell recording mode is determined by changes in the fluorescence intensity in cell-2 (ΔFI_2) over the time interval (Δt) and dye leakage to patch pipette-2 so that,

$$J_j = k[(vol_2 \Delta FI_2/\Delta t) + P_p FI_2] \quad [1]$$

where vol_2 is the volume of cell-2 and P_p is the permeability characterizing dye leakage from cell-2 to pipette-2. We assumed that dye concentration in pipette-2 is equal to zero due to its relatively high volume compared with the cell volume. Permeability is determined as the ratio of the flux to the driving force, which involves both the concentration gradient and the electric field for a charged molecule. To calculate the total junctional permeability (P_j) of GJs, we used a modified Goldman-Hodgkin-Katz (GHK) equation (21) describing electrodiffusion,

$$P_j = \frac{[(vol_2 \Delta FI_2/\Delta t) + P_p FI_2][1 - \exp(-zFV_j/RT)]}{(zFV_j/RT)[FI_1 - FI_2 \exp(-zFV_j/RT)]} \quad [2]$$

where z is the net charge of the dye molecule, F is Faraday's constant, R is the gas constant, T is the absolute temperature, and FI_1 and FI_2 are the fluorescence intensities in cell-1 (dye-

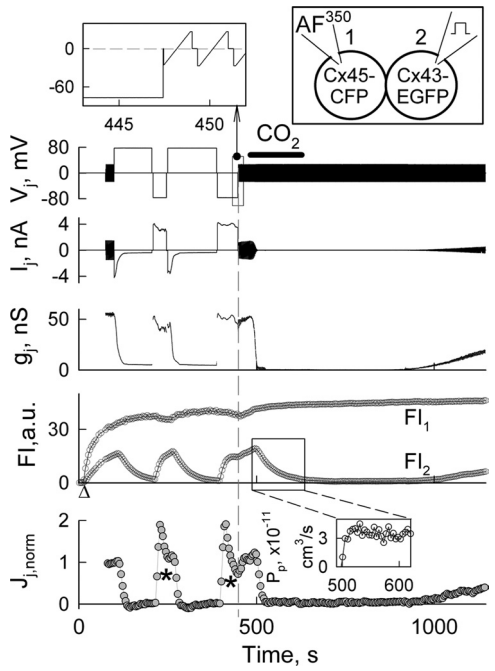

Fig. 3. Dye transfer modulation by V_j steps. Electrophysiological and fluorescence imaging recordings in a HeLaCx43-EGFP/HeLaCx45-CFP cell pair. The V_j trace shows the voltage protocol applied to the Cx43-EGFP expressing cell-2. The Cx43-CFP expressing cell-1 was loaded with AF^{350} (see *Top-Right* diagram). Repeated V_j ramps of ± 25 mV applied before and after voltage steps of ± 80 mV were used to measure g_j *(Top-Left Inset)*. FI_1 and FI_2 traces show the dynamics of AF^{350} fluorescence in cell-1 and cell-2, respectively. CO_2 application (horizontal bar) was used to block GJs and calculate P_p (*Bottom-Right Inset*). The $J_{j,norm.}$ trace shows the normalized total junctional flux. The asterisks indicate times when slow decay of $J_{j,norm}$ was caused mainly by a reduction in the difference between FI_1 and FI_2. Δ indicates moment of patch opening in cell-1.

donor) and cell-2 (dye-recipient), respectively. P_p was calculated from the dynamics of FI_2 decay after g_j was blocked by CO_2 or alkanols and using equation $P_p = -vol_2(\Delta FI_2/\Delta t)/FI_2$. Typically, the decay of FI_2 was close to exponential (see FI_2 traces in Fig. 2*B*, Fig. 3 and Fig. 6). P_p depends mainly on the size of the open patch at the very tip of the patch pipette, and in this experiment, P_p was $\approx 1.3 \times 10^{-11}$ cm^3/s. The single channel flux (J_γ) or permeability (P_γ) can be found by dividing J_j or P_j by the number of functional channels, $N_f = g_j/\gamma$, where γ is the single channel conductance, i.e., $J_\gamma = J_j(\gamma/g_j)$ and $P_\gamma = P_j(\gamma/g_j)$. See (*SI Appendix*) for more details about all equations used in this study. In accordance with an earlier report of Verselis et al. (2) the measured value of P_j at $V_j \approx 0$ mV ($P_{j,0}$) would be as follows:

$$P_{j,0} = \frac{[(vol_2 \Delta FI_2/\Delta t) + P_P FI_2]}{[FI_1 - FI_2]} \qquad [3]$$

In the experiment shown in Fig. 2*B*, J_γ of negatively charged AF^{350} (calculated using Eq. **1** divided by N_f and normalized with $J_{\gamma 0}$ measured just before the first positive V_j step, $J_{\gamma,norm}$) is modulated during V_j steps. Fig. 2*B* shows that positive V_j steps caused a ≈60% reduction, whereas negative V_j steps caused a ≈30% increase in $J_{\gamma,norm}$. Despite changes in $J_{\gamma,norm}$, P_γ (calculated using Eq. **2** divided by N_f) values boxed into gray squares remained constant during V_j steps (Fig. 2*B*). This suggests that the GHK equation used is applicable to describe permeability through GJs for at least V_js of ≈±20 mV. During repeated V_j ramps of small amplitude, P_γ was calculated using Eq. **3** divided by N_f. Fig. 2*B* show that on average $P_\gamma = 82.6 \pm 4.8 \times 10^{-15}$ cm^3/s ($n = 4$), which is close to the P_γ previously reported for Cx43-EGFP (20). In summary, in all five experiments we obtained data similar to those shown in Fig. 2*B* demonstrating that dye transfer can be accelerated or decelerated by ionophoresis, whereas P_γ remains unaffected in the absence of V_j-gating.

Dye Transfer Modulation in the Presence of V_j-Gating. Because we showed that Cx43/Cx45 heterotypic junctions exhibit V_j-gating and electric cell-to-cell signaling asymmetries (Fig. 1*B*), we hypothesized that these asymmetries should cause an asymmetry of J_j-V_j and P_j-V_j dependencies. To address this, we examined the effect of V_j on dye transfer in HeLa cells forming Cx43/Cx45 heterotypic GJs.

Fig. 3 shows an example of combined electrophysiological and fluorescence imaging recordings in a Cx43-EGFP/Cx45-CFP cell pair (see diagram). Initially, the patch was open in cell-2. After opening the patch in cell-1, FI started rising in cell-1 and with slower kinetics in cell-2. Repeated ramps of ± 25 mV were used to measure g_j before and after voltage steps of ± 80 mV were applied to cell-2. Initially g_j was ≈55 nS, but it decayed rapidly after applications of positive voltage steps to Cx43-EGFP cell reaching a steady state at $g_j = \approx 5$ nS (see g_j trace). During negative voltage steps, g_j recovered quickly followed by a ≈20% decay. These g_j changes are in agreement with the V_j-gating asymmetry shown in Fig. 1*B*. CO_2 application for ≈2 min induced transient uncoupling. From FI_2 changes shortly after CO_2 application, we found that $P_p = 3.8 \cdot 10^{-11}$ cm^3/s. J_j was calculated using Eq. **1** and normalized with J_{jo} measured just before the first positive V_j step (see $J_{j,norm}$ trace). During positive V_j steps, $J_{j,norm}$ declined to zero even though cells remained coupled with $g_j = \approx 5$ nS. $J_{j,norm}$ recovered rapidly during voltage steps of negative polarity. The decay of $J_{j,norm}$ to zero during positive V_j steps occurred despite the fact that positive voltage applied to the Cx43-EGFP expressing cell should increase the transfer of negatively charged AF^{350} molecules, suggesting that positive V_j steps drove the channels to a non-permeable substate. During negative V_j steps, the slow decrease in $J_{j,norm}$ (see asterisks) is presumably due to the reduction in the difference between FI_1 and FI_2. Similar data were obtained in seven other cell pairs forming Cx43-EGFP/Cx45-CFP and Cx43-EGFP/Cx45WT GJs. All collected data show that dye flux through Cx43/Cx45 heterotypic GJs can be modulated effectively by V_j-gating. As seen in Fig. 3, g_j does not reach a zero level at positive V_j steps. This is caused by the so called residual conductance resulting from the inability of the fast gating mechanism to close the GJ channel fully (22). Earlier, we and others reported that GJ channels closed to the residual state become impermeable to AF^{350}, Lucifer yellow (LY) and cAMP, while remaining permeable to small ions, major charge carriers for electrical cell–cell coupling (23, 24). In concert with those reports, in Fig. 3, $J_{j,norm}$ reached a zero level despite the fact that g_j is still ≈5 nS. We did not calculate P_γ for this experiment because an estimation of the numbers of functional channels can be under evaluated due to an effect of series resistance on g_j measurements at high g_js (≈60 nS) (25). We evaluated P_γ for Cx43/Cx45 heterotypic GJ channel from the experiments shown in Figs. 4 and 6 exhibiting relatively low g_js (see below).

What Is the Minimal V_j That Can Affect Dye Transfer? To answer this question, we examined the transfer of AF^{350} by applying relatively small V_j steps. Fig. 4 shows an experiment in which consecutive V_j steps of −14, −9, +9, −30, and −60 mV elicited V_j-gating and modulation of P_j (calculated using Eq. **2**). During repeated V_j ramps we assumed that $V_j = 0$ mV, and P_j was calculated using Eq. **3**. In this experiment, we used cells expressing Cx45WT (see diagram) instead of Cx45-CFP to show that CFP does not change the asymmetry of P_j-V_j dependencies. Repeated ±10 mV V_j ramps were applied in between V_j steps to

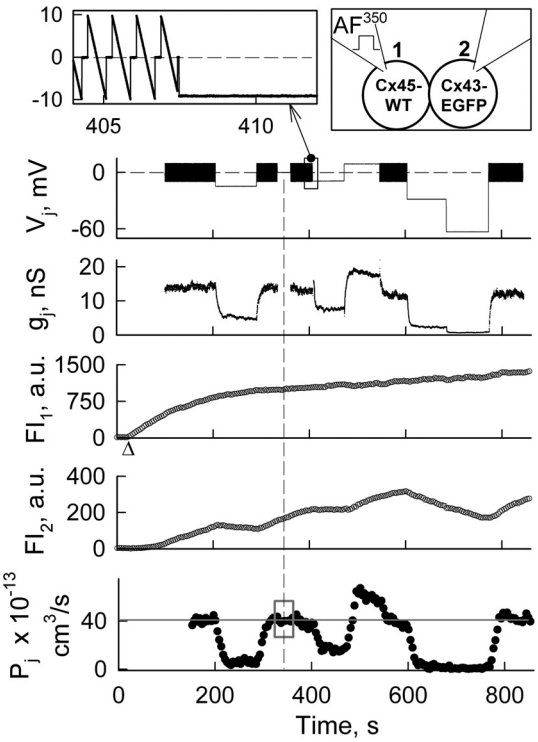

Fig. 4. Dye transfer modulation by small V_js. Electrophysiological and fluorescence imaging recordings in a HeLaCx43-EGFP/HeLaCx45WT cell pair. V_j trace shows the voltage protocol applied to the Cx45-expressing cell-1 (loaded with AF^{350}, see *Top-Right* diagram). Repeated V_j ramps of ± 10 mV (*Top-Left Inset*) were used to measure g_j in between V_j steps. FI_1 and FI_2 are fluorescence intensities measured in cell-1 and cell-2, respectively. The P_j trace shows the total junctional permeability. On average, during repeated small amplitude V_j ramps, P_j = ≈39.6 × 10^{-13} cm^3/s (gray line). Δ indicates moment of patch opening in cell-1.

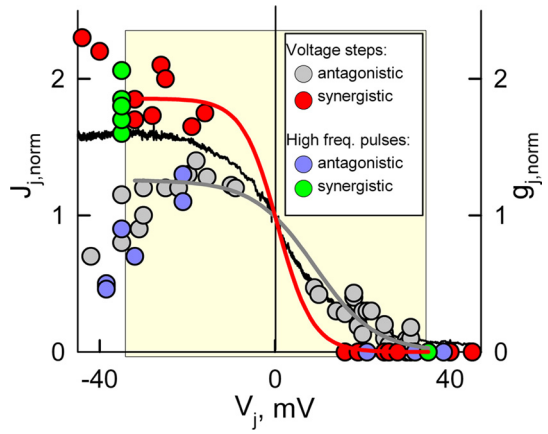

Fig. 5. Summarized data of J_j-V_j for AF^{350} measurements in 25 Cx43/Cx45 cell pairs. Data were normalized to J_j at V_j = 0 mV. Red (synergistic) and gray (antagonistic) circles indicate experimental data in which V_j steps of negative or positive polarity were applied to either cell of the cell pair. Red and gray curves show fitting of the data encompassed in the yellow square and shown in red and gray circles, respectively, by a sigmoidal equation. Green (synergistic) and blue (antagonistic) filled circles indicate experimental data in which high frequency bursts of pulses of positive polarity were applied to either cell of the cell pair (V_j was positive when the Cx43 cell was stimulated and negative when the Cx45 cell was stimulated, see Fig. 6). The data presented show that J_j dependence on V_j in experiments with synergistic action of ionophoresis and V_j-gating (red and green filled circles) is steeper around V_j = 0 mV than in experiments with antagonistic action of ionophoresis and V_j-gating (gray and blue filled circles). The black line shows normalized g_j-V_j plot, averaged from five experiments.

measure g_j, which was ≈14 nS. After ≈330 s, V_j ramps were not applied for ≈30 s to verify that they did not change P_j (see gray square on P_j trace). During these 30 s we calculated P_j using Eq. **3**. During all consecutive V_j steps of negative polarity (−14, −9, −30, and −60 mV), g_j decreased but some residual conductance still remained with g_js of ≈4, 8, 2, and 0.3 nS, respectively. At the same time, P_j decreased ≈80, 55, 95 and 100%, respectively. During a V_j step of +9 mV, g_j and P_j increased ≈30%. From P_j and g_j measurements at the beginning of the record and assuming that for Cx43/Cx45 channel γ = 55 pS (7), we found that $P_{\gamma,Cx43/Cx45} = P_j(\gamma/g_j)$ = ≈15 × 10^{-15} cm^3/s, which is in good agreement with earlier estimates of $P_{\gamma,Cx43/Cx45}$ at V_j ≈0 mV (20).

Thus, our data show that in Cx43/Cx45 junctions, V_js as low as ≈±10 mV can substantially modulate transfer of metabolites comparable in size with the dyes used (≈400 Da). This modulation of charged molecules can be amplified or reduced depending on whether V_j-gating and ionophoresis act synergistically or antagonistically. If a Cx43-expressing cell is loaded with AF^{350} and subjected to positive or negative V_j steps up to ≈30 mV, then g_j should be reduced or increased and V_j should decelerate or accelerate transfer of AF^{350}, respectively. Thus, at both V_j polarities, V_j-gating and ionophoresis should act on dye transfer synergistically. On the contrary, if a Cx45-expressing cell is loaded with AF^{350}, then V_j-gating and ionophoresis should affect dye transfer antagonistically. Data summarized from 24 cell pairs in Fig. 5 show the synergistic and antagonistic normalized J_j-V_j dependencies observed when cells expressing Cx43 or Cx45, respectively, were loaded with AF^{350}; data were normalized in respect to J_j at V_j≈0 mV. Red (synergistic) and gray (antagonistic) circles indicate experimental data in which V_j steps of negative or positive polarity were applied to either cell of the pair. Red and gray curves show fitting of the data encompassed in the yellow square and shown in red and gray circles, respectively, to a sigmoidal formula, $J_j = a/(1+\exp(-(V_j-V_o)/b))$. The major goal of this fitting was to evaluate the difference in steepness of J_j changes ($\Delta J_j/\Delta V_j$) at V_js around V_j = 0 mV. We found that coefficient b determining $\Delta J_j/\Delta V_j$ was equal to −4.2 ± 0.5 mV and −6.9 ± 0.6 mV for synergistic and antagonistic J_j-V_j dependence, respectively. Consequently, on average, $\Delta J_j/\Delta V_j$ was equal to ∼−0.09 and −0.03 normalized units of J_j per mV for synergistic and antagonistic dependencies, respectively. Therefore, V_js as small as ≈10 mV around V_j = 0 mV can cause substantial changes in J_j and these changes are ≈3-fold bigger under synergistic versus antagonistic action of ionophoresis and V_j-gating. In Fig. 5, the black line shows the normalized g_j-V_j dependence averaged from five g_j-V_j plots. Synergistic J_j-V_j dependence was more whereas antagonistic one was less steep than g_j-V_j dependence at V_j≈0 mV.

Dye Transfer Modulation by V_j Steps Repeated with High Frequency. Here, we examined whether dye transfer through heterotypic junctions can be modulated by series of V_j pulses resembling bursts of action potentials (APs) similar to those shown in Fig. 1*C*. In these experiments, we used only positive pulses because APs generated by excitable cells are generally positive, and we examined P_j during stimulation of either cell expressing Cx45 or Cx43. Fig. 6 shows recordings of voltage (V_1 and V_2) and FI (FI_1 and FI_2) and P_j. Cell-1 expressing Cx45WT was loaded with AF^{350} (see diagram). Initially, repeated small ramps were applied in cell-2 to measure g_j, which was ≈3.5 nS. In response to repeated (50 Hz) pulses of 60 mV in amplitude and 10 ms in duration applied to cell-2, g_j decayed and over a ≈4 s period reached a steady state of ≈0.2 nS. Subsequently, when a burst of pulses was applied to cell-1, g_j increased to ≈6.5 nS followed by

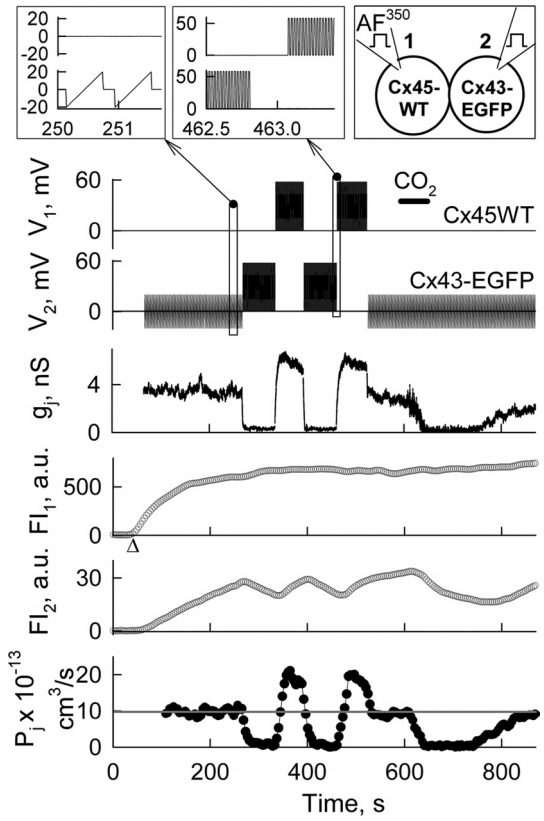

Fig. 6. Dye transfer modulation by bursts of + 60 mV pulses 10 ms in duration repeated at 50 Hz frequency *(Top-Middle Inset)*, and applied alternately to cell-1 and cell-2 of a HeLaCx43-EGFP/HeLaCx45WT cell pair *(Top-Right* diagram). V_1 and V_2 traces show voltage protocols applied in cell-1 (loaded with AF^{350}) and cell-2, respectively. Repeated V_j ramps of ± 20 mV applied in cell-2 *(Top-Left Inset)* were used to measured I_j and calculate the g_j trace. Fl_1 and Fl_2 traces show dynamics of dye fluorescence in cell-1 and cell-2, respectively. The P_j trace shows the total junctional permeability. On average, at $V_j = 0$ mV, $P_j = \approx 9.9 \times 10^{-13}$ cm^3/s (gray line). During series of pulses, P_j was calculated using Eq. **2** at $V_j = 21$ mV, i.e., ≈35% of 60 mV pulses. CO_2 application (horizontal bar) was used to block GJs and calculate P_p. Δ indicates moment of patch opening in cell-1.

decay over ≈5 s to ≈5.5 nS, suggesting that more GJ channels were open during this period of stimulation. To find P_p, cells were fully uncoupled with a short application of CO_2. During small V_j ramps, P_j was calculated using Eq. **3**. During V_j pulses, P_j was calculated using Eq. **2**. Assuming a linear relationship between P_j and g_j ($P_j = P_{j,0}(g_j/g_{j,0})$, were $g_{j,0}$ is the conductance at control conditions), then by examining P_js at different V_js, we found that P_j increases 1.9-fold at $V_j = 21$ mV, i.e., ≈35% of 60 mV pulses (see P_js shown in filled circles).

Single channel permeability estimates in this experiment using the same procedure as we did for data shown in Fig. 4 resulted to $P_{\gamma,Cx43/Cx45} = \approx 14 \times 10^{-15}$ cm^3/s, which is close to values obtained from Fig. 4 and reported earlier for $V_j \approx 0$ mV (20).

Thus, high frequency stimulation of the Cx43-EGFP expressing cell blocked AF^{350} transfer whereas stimulation of the Cx45 expressing cell increased both g_j and P_j equally if V_j was equal 35% of the amplitude of pulses. Green (synergistic) and blue (antagonistic) circles in Fig. 5 indicate experimental data in which a high frequency burst of pulses of positive polarity were applied to either cell of the cell pair (V_j positive when Cx43 cell was stimulated and *v.v.*). Data shown in green and blue circles were not included in the fitting process but, in general, they show that application of V_j steps or high frequency bursts of pulses result in similar effects on J_j.

In summary, these data show that dye transfer of AF^{350} in Cx43/Cx45 GJs can be enhanced or reduced depending whether APs first arrive in the cell expressing Cx43 or Cx45. Similar data were obtained in five other Cx43/Cx45 cell pairs by using AF^{350}. Comparable results were obtained in Cx43-EGFP/Cx45-CFP cell pairs using LY instead of AF^{350} (Fig. S1).

Discussion

We have demonstrated that V_j can increase or fully block cell–cell transfer of dye molecules comparable in size and net charge with many metabolites and signaling molecules indicating that the data apply to metabolic cell–cell communication and intercellular signaling. We found that V_j steps as small as ≈10 mV as well as series of pulses of high frequency resembling bursts of APs can modulate to a large extent metabolic communication through GJs exhibiting V_j-gating asymmetry.

Transfer of charged molecules is affected by ionophoresis and V_j-gating. Ionophoresis affects cell–cell transfer of charged metabolites independent of connexin type and whether GJ channels are homotypic, heterotypic or heteromeric. Our data show that the modified GHK equation used predicts P_γ for negatively charged AF^{350} at V_js up to at least ≈±20 mV (Fig. 2). This may not necessarily be true for larger molecules or higher V_js due to: (*i*) breakdown of ionic independence, (*ii*) electrostatic interaction with the channel's wall, etc.

For a long time, scientists working in the gap junction field have been asking, why there is a need for voltage-dependent gating of connexins expressed in non-excitable tissues such as hepatocytes, astrocytes and epithelial cells. Although these cells do not generate action potentials that can lead to large V_js between adjacent cells and trigger V_j-gating, we demonstrate that even relatively small differences in the resting potential between adjacent cells (≈10 mV) can substantially modulate transfer of metabolites and this effect is augmented in heterotypic gap junctions. Can such V_js be physiologically relevant? The resting potential (V_R) varies among different cell types in broad ranges exceeding tens of mV under normal conditions, and even more under pathological conditions when cells lose their electrochemical gradients. It has been shown that astrocytes, which are well coupled through gap junctions, exhibit a wide range of V_Rs from −22 to −82 mV, and exhibit spontaneous changes of their V_Rs under different physiological conditions (26). Numerous studies have shown that hypoxia, ischemia, hyperkalemia or similar conditions that damage energetic and ionic homeostasis result in alteration of V_Rs. Depending upon the severity of ischemic or hypoxic conditions, changes in V_R can be far greater than 10 mV (27). Thus, even in cells that have the same V_R under normal conditions, changes in their network profile or local ischemia can form differences in V_R (ΔV_R) and consequently modulate metabolic communication by ionophoresis in all types of GJs and, in addition, by V_j-gating if cells are coupled through heterotypic GJs. It is important to note that actual ΔV_R depend on the intrinsic V_Rs of communicating cells, coupling strength and their input resistance. We assume that ΔV_Rs even <10 mV can be effective because they can be long-lasting. If ΔV_R were positioned on a g_j-V_j plot of Cx43/Cx45 heterotypic junction as the working point (WP), then changing ΔV_R would move the WP along the V_j axis and cause substantial changes in g_j and J_j (see Fig. S2).

As reported, GJ channels operated by the fast gating mechanism close to the residual state that remains permeant for small ions but restricts permeation of more complex molecules such as AF^{350}, LY and cAMP (22, 24). Therefore, P_j-V_j dependence can exhibit even higher asymmetry than g_j-V_j dependence and V_j can modulate metabolic communication more effectively than g_j. This asymmetry can be enhanced by synergistic action of ionophoresis and V_j-gating (Fig. 5) to the degree that ΔV_Rs as small as 5–10 mV can substantially modulate metabolic communication.

For more details about theoretically predicted changes of J_j, versus V_j see *SI Appendix* and Fig. S3.

V_j-gating under physiological conditions can also take place in electrically excitable tissues during the spread of excitation. It was shown that V_j arising on the front of excitation spread can dynamically reduce g_j and may play a role in the development of cardiac arrhythmias (28). Electrical activity during cardiac arrhythmias resembles bursts of APs similar to those in Fig. 1*C* that may cause profound changes of g_j and P_j. Similar instances can occur between neurons that express or coexpress mCx30.2, Cx36 and Cx45 (14). Dynamic changes in g_j can also occur when only one of the coupled cells is excitable, as at GJs between neurons and astrocytes, between endothelium and smooth muscle cells in blood vessels, etc. All these systems coexpress Cx45 in parallel with Cx31, Cx36, Cx40, Cx43 and/or Cx47 that can form heterotypic junctions exhibiting V_j-gating asymmetry. In the heart, fibroblasts that are not excitable express Cx45 (29) and are coupled with cardiomyocytes preferentially expressing Cx43. Fibroblasts, exhibiting relatively small V_R, will be more depolarized than cardiomyocytes during the repolarisation phase. Thus, most of Cx43/Cx45 GJs should open and cells should be able to exchange metabolites. During APs when the membrane potential of cardiomyocytes becomes positive, Cx43/Cx45 channels should close resulting in the reduction of g_j, P_j and the "sink" effect of the fibroblasts' network on the excitation of cardiomyocytes thereby enhancing the safety factor for the spread of excitation in the syncytial network of cardiomyocytes. During the rest of the cardiac cycle, g_j should increase to a degree that fibroblasts may help cardiomyocytes to restore their energetic and ionic balance.

In summary, we demonstrate that long-lasting V_js of small amplitude or series of V_j pulses resembling bursts of APs can modulate dye transfer with high efficacy suggesting that heterotypic GJs may act as voltage-dependent regulatory valves for intercellular signaling. Movie S1 demonstrates modulation of dye transfer by voltage steps over 20 min of time-lapse imaging. The regulation of metabolic communication and intercellular signaling by V_j can play a crucial role in many aspects of normal physiology, embryonic development, and tissue regeneration. In addition, the role of GJs can be substantially enhanced under pathological conditions when intercellular gradients of nutrients and signaling molecules are increased. Thus, we describe a general phenomenon of the modulation of intercellular electrical and chemical signaling by voltage that may have a broad impact on cellular and tissue function.

Methods

SI Appendix includes details of the experimental procedures and equations. Experiments were performed on HeLa cells transfected with wild type Cx43 and Cx45 and their fusion forms with color variants of green fluorescent proteins (EGFP or CFP) tagged to the C terminus. Junctional conductance (g_j) was measured using the dual whole-cell voltage clamp method (9). For dye transfer studies, a given fluorescent dye was introduced into cell-1 of a cell pair through a patch pipette in whole-cell voltage clamp mode and the fluorescence intensity of dye was measured in cell-1 and cell-2. Dyes used include (molecular mass of the fluorescent ion, valence): Alexa Fluor-350 (AF^{350}) (326, −1) and Lucifer yellow (LY) (443, −2) (Invitrogen, Eugene, OR). For calculation of the total junctional permeability (P_j) we used the Goldman-Hodgkin-Katz (GHK) equation (21) already used earlier for P_j studies by Verselis et al. (2). We modified this equation allowing for P_j evaluation during combined fluorescence imaging and g_j recordings when there is constant dye leakage from cell-2 to the patch pipette-2.

ACKNOWLEDGMENTS. We thank Dr. Vytautas K. Verselis and Dr. Mindaugas Rackauskas for discussions and help at an initial stage of this project, Dr. Michael V. L. Bennett for helpful comments and remarks, and Angele Bukauskiene for excellent technical assistance. This work was supported by National Institutes of Health Grants RO1 NS036706 and RO1HL084464 (to F.F.B.).

1. Sohl G, Maxeiner S, Willecke K (2005) Expression and functions of neuronal gap junctions. *Nat Rev Neurosci* 6:191–200.
2. Verselis V, White RL, Spray DC, Bennett MVL (1986) Gap junctional conductance and permeability are linearly related. *Science* 234:461–464.
3. Neijssen J, et al. (2005) Cross-presentation by intercellular peptide transfer through gap junctions. *Nature* 434:83–88.
4. Valiunas V, et al. (2005) Connexin-specific cell-to-cell transfer of short interfering RNA by gap junctions. *J Physiol* 568:459–468.
5. Bedner P, et al. (2006) Selective Permeability of Different Connexin Channels to the Second Messenger Cyclic AMP. *J Biol Chem* 28:6673–6681.
6. Harris AL (2001) Emerging issues of connexin channels: Biophysics fills the gap. *Q Rev Biophys* 34:325–427.
7. Bukauskas FF, Bukauskiene A, Verselis VK, Bennett MVL (2002) Coupling asymmetry of heterotypic connexin 45/connexin 43-EGFP gap junctions: Properties of fast and slow gating mechanisms. *Proc Natl Acad Sci USA* 99:7113–7118.
8. Abrams CK, et al. (2006) Properties of human connexin 31, which is implicated in hereditary dermatological disease and deafness. *Proc Natl Acad Sci USA* 103:5213–5218.
9. Rackauskas M, et al. (2007) Gating properties of heterotypic gap junction channels formed of connexins 40, 43 and 45. *Biophys J* 92:1952–1965.
10. Kreuzberg MM, Willecke K, Bukauskas F (2006) Connexin-Mediated Cardiac Impulse Propagation: Connexin 30.2 Slows Atrioventricular Conduction in Mouse Heart. *Trends in Cardiovasc Med* 16:266–272.
11. Bruzzone R, Haefliger JA, Gimlich RL, Paul DL (1993) Connexin40, a component of gap junctions in vascular endothelium, is restricted in its ability to interact with other connexins. *Mol Biol Cell* 4:7–20.
12. Li X, Simard JM (2001) Connexin45 gap junction channels in rat cerebral vascular smooth muscle cells. *Am J Physiol Heart Circulatory Physiol* 281(5):H1890–H1898.
13. Kreuzberg MM, et al. (2005) Functional properties of mouse connexin30.2 expressed in the conduction system of the heart. *Circ Res* 96:1169–1177.
14. Kreuzberg MM, et al. (2008) Expression of connexin30.2 in interneurons of the central nervous system in the mouse. *Mol Cell Neurosci* 37:119–134.
15. Rozental R, et al. (2001) Gap junction-mediated bidirectional signaling between human fetal hippocampal neurons and astrocytes. *Dev Neurosci* 23(6):420–431.
16. Paulauskas N, Pranevicius M, Pranevicius H, & Bukauskas FF (2009) A four-state model of contingent gating of gap junction channels containing two ''fast'' gates sensitive to transjunctional voltage. *Biophys J* 96:3936–3948.
17. Harris AL, Spray DC, Bennett MVL (1983) Control of intercellular communication by voltage dependence of gap junctional conductance. *J Neurosci* 3:79–100.
18. Goldberg GS, Valiunas V, Brink PR (2004) Selective permeability of gap junction channels. *Biochim Biophys Acta* 1662:96–101.
19. Ek-Vitorin JF, Burt JM (2005) Quantification of gap junction selectivity. *Am J Physiol Cell Physiol* 289:C1535–C1546.
20. Rackauskas M, Verselis VK, Bukauskas FF (2007) Permeability of homotypic and heterotypic gap junction channels formed of cardiac connexins mCx30.2, Cx40, Cx43, and Cx45. *Am J Physiol Heart Circ Physiol* 293(3):H1729–H1736.
21. Hille B (2001) *Ionic Channels of Excitable Membranes* (Sinauer Associates, Sunderland, MA).
22. Bukauskas FF, Verselis VK (2004) Gap junction channel gating. *Biochim Biophys Acta* 1662:42–60.
23. Bukauskas FF, Bukauskiene A, Verselis VK (2002) Conductance and permeability of the residual state of connexin43 gap junction channels. *J Gen Physiol* 119:171–186.
24. Qu Y, Dahl G (2002) Function of the voltage gate of gap junction channels: Selective exclusion of molecules. *Proc Natl Acad Sci USA* 99:697–702.
25. Wilders R, Jongsma HJ (1992) Limitations of the dual voltage clamp method in assaying conductance and kinetics of gap junction channels. *Biophys J* 63:942–953.
26. McKhann GM, 2nd RDA, Janigro D (1997) Heterogeneity of astrocyte resting membrane potentials and intercellular coupling revealed by whole-cell and gramicidin-perforated patch recordings from cultured neocortical and hippocampal slice astrocytes. *J Neurosci* 17:6850–6863.
27. Hyllienmark L, Brismar T (1999) Effect of hypoxia on membrane potential and resting conductance in rat hippocampal neurons. *Neuroscience* 91:511–517.
28. Lin X, Gemel J, Beyer EC, Veenstra RD (2005) Dynamic model for ventricular junctional conductance during the cardiac action potential. *Am J Physiol Heart Circ Physiol* 288:H1113–H1123.
29. Camelliti P, Green CR, LeGrice I, Kohl P (2004) Fibroblast network in rabbit sinoatrial node: structural and functional identification of homogeneous and heterogeneous cell coupling. *Circ Res* 94:828–835.